Informatik aktuell

T. Tolxdorff T. M. Deserno
H. Handels H.-P. Meinzer
(Hrsg.)

Bildverarbeitung für die Medizin 2016

Algorithmen
Systeme
Anwendungen

Proceedings des Workshops
13. bis 15. März 2016 in Berlin

Springer Vieweg

Detection and Quantification of Cytoskeletal Granules

Dennis Eschweiler[1], Jakob Unger[1], Kraisorn Chaisaowong[2], Mugdha Sawant[3], Reinhard Windoffer[3], Rudolf E. Leube[3], Dorit Merhof[1]

[1]ACTIVE Center, Institute of Imaging and Computer Vision, RWTH Aachen University
[2]Department of Electrical and Computer Engineering, Faculty of Engineering, King Mongkut's University of Technology North Bangkok
[3]Institute of Molecular and Cellular Anatomy, Uniklinik RWTH Aachen
dennis.eschweiler@rwth-aachen.de

Abstract. The cytoskeleton is a dynamic scaffolding maintaining cell stability and motility. Keratin filaments form cytoskeletal networks in the cytoplasm of epithelial cells. Genetic mutations of keratin genes have been implicated in human skin diseases, such as epidermolysis bullosa simplex. Keratin network organization is severely impaired in these instances resulting in the formation of prominent granular aggregates. To gain an understanding of the pathomechanisms underlying keratin granule formation and to screen for factors affecting this process, an automated segmentation routine of keratin granules is proposed in this paper. As such, the presented method holds a lot of potential for an objective assessment of keratin organization to improve treatment of genetic keratinopathies.

1 Introduction

The cytoskeleton is a main structural feature of eukaryotic cells determining cell shape and facilitating a variety of cell functions. It consists of extensive, interconnected three-dimensional networks that are composed of intermediate filaments (IFs), microtubules (MTs) and microfilaments (MFs). IFs represent the largest cytoskeletal gene family comprising about 70 genes, with 54 of them coding for keratin polypeptides. IFs not only fulfill scaffolding functions, but also form complex signaling platforms and interact with various kinases, cytoskeletal adaptors, and apoptotic proteins [1]. Genetic mutations in IF proteins account for a large number of diseases, ranging from skin fragility conditions to cardiomyopathies and premature aging.

Keratin filaments (KFs), composing IFs within epithelial cells, are connected to desmosomal cell-cell contact sites and to hemidesmosomal cell-substratum contacts, thereby forming a well-anchored supracellular scaffolding and stabilizing element of epithelial tissues. KFs are subject to a continuous cycle of assembly and disassembly consisting of multiple spatially defined steps [2]. Notably, KF networks are completely disassembled in some epithelial cell types

T. Tolxdorff et al. (Hrsg.), *Bildverarbeitung für die Medizin 2016*,
DOI 10.1007/978-3-662-49465-3_46,

forming prominent granular aggregates at the onset of mitosis. Subsequent network reformation occurs after cell division and proceeds predominantly from the cell periphery coincident with granule dissolution.

Remarkably, keratin granules are also formed when mutant keratin reporters are expressed in cultured cells (Fig. 1). Single point mutations in keratin genes have been linked to blister-forming epidermal diseases, most notably in epidermis bullosa simplex [3, 4]. In cells producing such mutant keratins, short-lived granules are formed from keratin particles that nucleate in the cell periphery. These granules are moved toward the cell interior and rapidly disassemble. Only an incomplete filamentous network is detected in these cells that is mostly localized in the perinuclear region.

The examples illustrate that the formation of motile and instable keratin granules is a stereotypical response to "out-of-balance" situations in epithelial cells. Thus, quantification of this reaction in relation to endogeneous network formation is highly desirable to assess keratin organization as a reflection of altered epithelial function. While recent literature focuses on quantitative analysis of filament network topology and dynamics [5, 6], keratin granule formation has not been addressed yet. Towards this goal, we propose a method to detect keratin granules in fluorescence microscopic images using an anisotropic 2D Gaussian model.

2 Material and method

2.1 Image acquisition and data

In order to visualize K5 keratin structures and their dynamics in cultured cells (type II keratin knockout murine keratinocytes [7]), fluorescent reporters were used, that were monitored by fluorescence microscopy. In the current study, fluorescence images were recorded with a CCD-camera mounted on a Zeiss Apo-Tome.2 wide-field microscope.

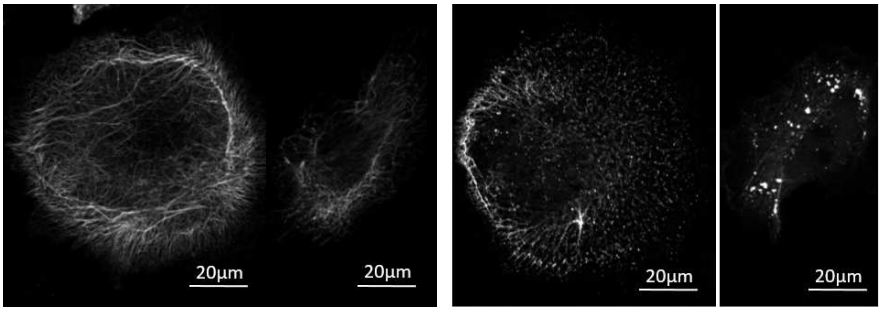

(a) (b)

Fig. 1. Keratin K5, which is prominent in basal regions of epidermis, shows an intact network structure (keratin expressed: WT K5 YFP)(a). Mutation of the K5 gene results in formation of granular aggregates with only few remaining filamentous structures (keratin expressed: T150D K5 YFP)(b).

To assess the precision of the segmentation routine, eleven images showing KFs and granules served as input data for evaluation. From these eleven images, 22 segments were extracted, each with a side length between 50 and 100 pixels and containing between zero and 30 granules. Within the image segments, all granules were manually segmented by an experienced cell biologist forming the ground truth for validation purposes. An example of an image segment and the corresponding ground truth is depicted in Fig. 3 (training set).

2.2 Adaption of an anisotropic Gaussian model

The resolution that can be achieved by conventional optical techniques is limited meaning that tightly packed molecules cannot be separated anymore. Their visual appearance is thus characterized by the point-spread function (PSF) which can be adequately modeled by a 2D Gaussian [8]. The visual appearance of a single keratin granule depends on the number and spatial arrangement of the corresponding fluorescent proteins. In this regard, granules are modeled as anisotropic Gaussian

$$\mathrm{G(x,y)} = \mathrm{a} + \mathrm{b} \cdot \exp\left[-\left(\frac{(\mathrm{x}-\mathrm{c_x})\cos\alpha + (\mathrm{y}-\mathrm{c_y})\sin\alpha}{\sigma_{\max}} \right)^2 - \left(\frac{-(\mathrm{x}-\mathrm{c_x})\sin\alpha + (\mathrm{y}-\mathrm{c_y})\cos\alpha}{\sigma_{\min}} \right)^2 \right] \quad (1)$$

where a and b denote offset and scaling, c_x and c_y the center coordinates, $\sigma_{\min}$ and $\sigma_{\max}$ the minimum and maximum standard deviations and α the angle of rotation representing the large variety of granule shapes.

To each granule that has been segmented by the expert, the Gaussian model (Eq. 1) is adapted using the trust-region algorithm [9] (Fig. 2). In this way, the model parameters $\mathrm{P_{fit}} = \{\sigma_{\max}, \sigma_{\mathrm{oval}} = \frac{\sigma_{\max}}{\sigma_{\min}}, \alpha, \rho\}$ can be identified for each manual segmentation where $\sigma_{\min}$, $\sigma_{\max}$ denote the maximum and minimum spread, α the angle and ρ the linear correlation coefficient between the segmented image and the adapted Gaussian function.

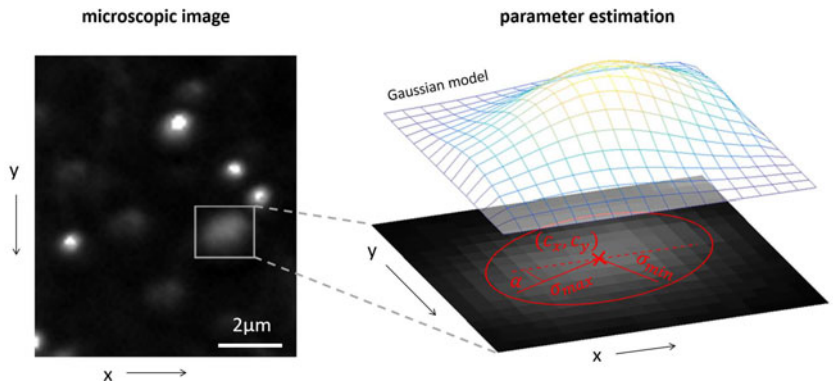

Fig. 2. The granules are adapted to an anisotropic 2D Gaussian model (1) using the trust-region algorithm.

2.3 Segmentation of keratin granules

The processing pipeline of the detection routine is depicted in Fig. 3 and can be summarized as follows:

a) The model is trained using a leave-one-image-out cross-validation scheme. From the training set of images and corresponding expert segmentations, the granules are subsequently fitted to the Gaussian model as described in Sect. 2.2.

b) By modifying the parameters of the Gaussian model (1), a catalog of template functions is generated that specifies the variety of granule shapes. From the training set, the model parameters P_{fit} are estimated for each segmented granule specifying upper and lower parameter bounds for the catalog templates.

c) A normalized cross-correlation is performed for each template of the catalog and the input image. Note that due to normalization, offset a and scaling b do not influence the correlation results and are thus not specified in P_{fit}. If the correlation coefficient ρ exceeds the threshold ρ_{thres} the elliptic area defined by the standard deviations $\sigma_{\max}$ and $\sigma_{\min}$ is labeled as granule.

d) Generally, keratin granules appear in different sizes. Larger accumulations of fluorescent proteins exhibit a rather large and bulky shape. Furthermore, they emit fluorescence of very high intensity. If the camera intensity range is exceeded, a flat plateau is built up due to a ceiling effect. The Gaussian model is thus not suitable for these clusters. Instead they are segmented using a simple threshold criterion followed by a morphologic opening to remove remaining noise artifacts.

The segmentation result is finally given by the union of the results of the cross-correlation and the cluster detection steps c) and d).

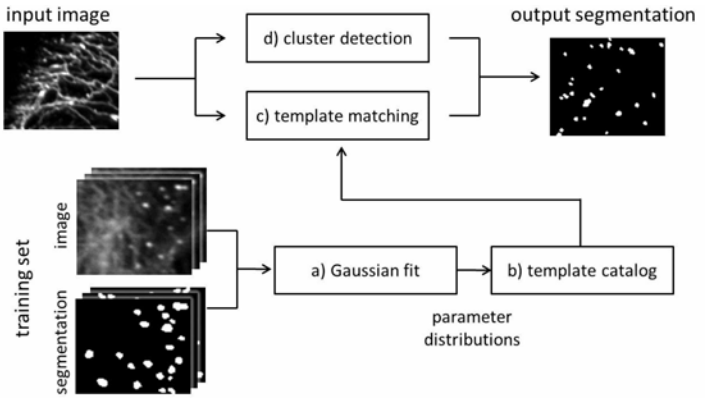

Fig. 3. Processing pipeline of the cytoskeletal granules segmentation procedure.

3 Results

Following a leave-one-image-out cross-validation scheme, the ranges of the parameters P_{fit} specifying the catalog of template functions are derived from the training data set. The lower bound of the maximum spread $\sigma_{\max}$ is set to the p-quantile of the distribution of the training set and equal to one for the ovality parameter σ_{oval} which also includes circular granule shapes. The upper bound of $\sigma_{\max}$ and σ_{oval} is given by the $(1 - \text{p})$-quantile of the training set. As the orientation of granules can be in arbitrary direction the entire parameter range $\alpha \in [0, \pi]$ is taken for the angle α. The correlation threshold ρ_{thres} is set to the k-quantile of the corresponding threshold distribution obtained from the training set.

By varying p, the segmentation process can be adapted to more or less diverse granule appearances whereas k affects the segmentation sensitivity. Granules are considered to be identified correctly if the overlapping area between automatic and expert segmentation exceeds 50% of their union. Parameter optimization is performed by maximizing the F_1-score, which led to an optimal setting for $\text{p} = 0.1$ and $\text{k} = 0.25$. Specifically, precision and recall of 0.864 and 0.896 were achieved. Fig. 4 shows an example of a wide-field fluorescence microscopic image (a) and the segmentation result using the optimal parameter bounds (b).

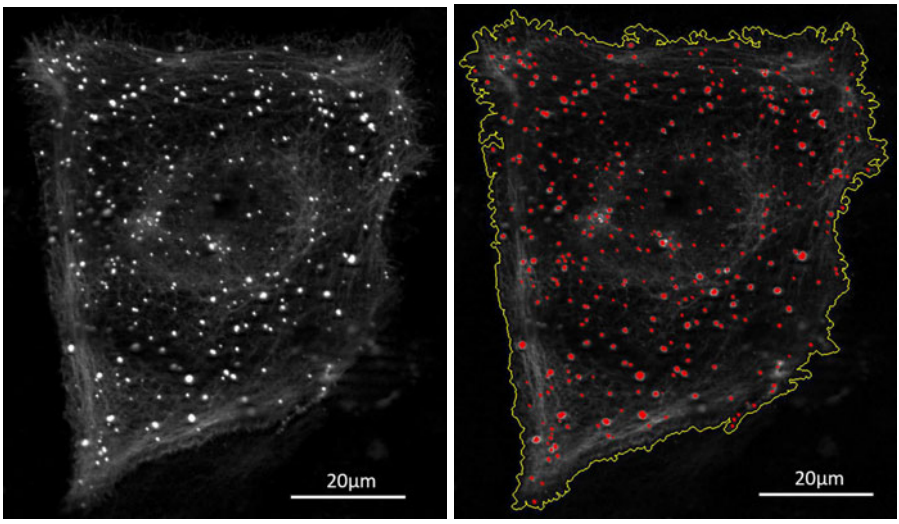

(a) (b)

Fig. 4. Keratin network and granules (a) acquired by wide-field fluorescence microscopy. Within the segmentation results (b) the granules are marked in red and the outer cell boundary is framed in yellow.

4 Discussion

In this contribution, a method for segmenting cytoskeletal keratin granules in wide-field fluorescence microscopic images has been presented. A high reliability was demonstrated providing the basis for a fully automated quantitative analysis. Minor errors were recognized for crossing filaments where localized intensity peaks can be erroneously labeled as granules.

The extension of the proposed method to three-dimensional images of fluorescently labeled keratin is straightforward. Processing 3D images could further enhance segmentation reliability since overlapping filaments could be distinguished more easily. The tools described in this manuscript will be valuable in screens for modifiers of keratin granule formation to improve treatment of genetic keratinopathies and to modulate keratin function in the context of epithelial disease.

Acknowledgement. This work was supported by the German Research Foundation (DFG), grant number ME3737/3-1.

References

1. Strnad P, Stumptner C, Zatloukal K, et al. Intermediate filament cytoskeleton of the liver in health and disease. Histochem Cell Biol. 2008;129(6):735–49.
2. Windoffer R, Beil M, Magin TM, et al. Cytoskeleton in motion: the dynamics of keratin intermediate filaments in epithelia. J Cell Biol. 2011;194:669–78.
3. Chamcheu J, Siddiqui I, Syed D, et al. Keratin gene mutations in disorders of human skin and its appendages. Arch Biochem Biophys. 2011;508:123–37.
4. Haines RL, Lane EB. Keratins and disease at a glance. J Cell Sci. 2012;125:3923–8.
5. Herberich G, Würflinger T, Sechi A, et al. Fluorescence microscopic imaging and image analysis of the cytoskeleton. Signals Syst Comput ASILOMAR. 2010; p. 1359–63.
6. Lichtenstein N, Geiger B, Kam Z. Quantitative analysis of cytoskeletal organization by digital fluorescent microscopy. Cytometry A. 2003;54A:8–18.
7. Kröger C, Loschke F, Schwarz N, et al. Keratins control intercellular adhesion involving PKC-α-mediated desmoplakin phosphorylation. J Cell Biol. 2013;201(5):681–92.
8. Zhang B, Zerubia J, Olivo-Marin JC. Gaussian approximations of fluorescence microscope point-spread function models. Appl Opt. 2007;46(10):1819–29.
9. Branch MA, Coleman MA, Li Y. A subspace, interior, and conjugate gradient method for large-scale bound-constrained minimization problems. SIAM J Sci Comput. 1999;21:1–23.